Measurement report: Distinct Emissions and Volatility Distribution of Intermediate Volatility Organic Compounds from on-road Chinese Gasoline Vehicle: Implication of High Secondary Organic Aerosol Formation Potential

Rongzhi Tang[1,2,#], Quanyang Lu[3,#], Song Guo[1,4,*], Hui Wang[1], Kai Song[1], Ying Yu[1], Rui Tan[1], Kefan Liu[1], Ruizhe Shen[1], Shiyi Chen[1], Limin Zeng[1], Spiro D. Jorga[3], Zhou Zhang[5], Wenbin Zhang[5], Shijin Shuai[5], Allen L. Robinson[3,*]

1 State Key Joint Laboratory of Environmental Simulation and Pollution Control, College of Environmental Sciences and Engineering, Peking University, Beijing, 100871, PR China

2 School of Environmental and Material Engineering, Yantai University, Yantai, 264003, PR China

3Department of Mechanical Engineering and Center for Atmospheric Particle Studies, Carnegie Mellon University, 5000 Forbes Avenue, Pittsburgh, Pennsylvania 15213, United States

4 International Joint Laboratory for Regional Pollution Control, Ministry of Education, Beijing, 100816, PR China

5 State Key Laboratory of Automotive Safety and Energy, School of Vehicle and Mobility, Tsinghua University, Beijing, 100084, PR China

Correspondence to: S. Guo songguo@pku.edu.cn, A. Robinson:alr@andrew.cmu.edu

[#]These authors contribute equally to this work

Abstract

In the present work, we performed chassis dynamometer experiments to investigate the emissions and secondary organic aerosol (SOA) formation potential of intermediate volatility organic compounds (IVOCs) from an on-road Chinese gasoline vehicle. High IVOCs emission factors (EFs) and distinct volatility distribution were recognized. The IVOCs EFs for the China V vehicle ranged from 12.1 to 226.3 mg kg-fuel^{-1}, with a median value of 83.7 mg kg-fuel^{-1}, which is higher than that from US vehicles. Besides, large discrepancy in volatility distribution and chemical composition of IVOCs from Chinese gasoline vehicle exhaust is discovered, with larger contributions of B_{14}-B_{16} compounds (retention time bins corresponding to C_{14}-C_{16} *n*-alkanes) and higher percentage of *n*-alkanes. Further we investigated the possible reasons that influence the IVOCs EFs and volatility distribution and found that fuel type, starting mode, operating cycles and acceleration rates did have an impact on the IVOCs EF. When using E10 (ethanol volume ratio of 10%, v/v) as fuel, the IVOCs EF of the tested vehicle was lower than that using commercial China standard V fuel. The average IVOC-to-THC ratios for gasoline-fueled and E10-fueled gasoline vehicle are 0.07 ±0.01 and 0.11 ±0.02, respectively. Cold-start operation has higher IVOCs EF than hot-start operation. Chinese Light vehicles Test Cycle (CLTC) produced 70% higher IVOCs than those from the World-wide harmonized Light-duty Test Cycle (WLTC). We found that the tested vehicle emitted more IVOCs at lower acceleration rates, which leads to high EFs under CLTC. The only factor that may influence the volatility distribution and compound composition is the engine-aftertreatment system, which has compound and volatility selectivity in exhaust purification. These distinct characteristics in EFs and volatility may result in higher SOA formation potential in China. Using published yield data and surrogate equivalent method, we estimated SOA formation under different OA loading and NO_x conditions. Results showed that under low and high NO_x conditions at different OA loadings, IVOCs contributes more than 80% of the predicted SOA. Furthermore, we built up a parameterization method to simply estimate the vehicular SOA based on our bottom-up measurement of VOCs and IVOCs, which would provide another

50   dimension of information when considering the vehicular contribution to the ambient

51   OA. Our results indicate that vehicular IVOCs contribute significantly to SOA,

52   implying that the importance of reducing IVOCs when making air pollution

53   controlling policies in urban area of China.

54

1 Introduction

Atmospheric fine particulate matter has great impacts on human health, climate, and global environmental issues (Tang et al., 2018; Guo et al., 2014b; Hallquist et al., 2009; Kanakidou et al., 2005). Organic aerosols are a major component of fine particulate matter. Secondary organic aerosol (SOA), formed from multiple generations of oxidation of thousands of organic gases and vapors, contribute 30% or more of organic aerosols in different areas of the world (Zhang et al., 2007). Due to its complexity in sources and photochemical processes, SOA formation remains uncertain (Tang et al., 2019; Guo et al., 2014a).

A large discrepancy remains between modeled and measured SOA. One possible reason is missing SOA precursors. Apart from traditional SOA precursors, i.e. volatile organic compounds (VOCs), Robinson et al. (2007) proposed intermediate volatility organic compounds (IVOCs) as important contributors to SOA formation. IVOCs are less volatile than VOCs with effective saturation concentrations in the range of 10^3 to 10^6 μg/m^3(Donahue et al., 2006), roughly corresponds to the volatility range of C_{12}-C_{22} n-alkanes. IVOCs exist mainly in the gas phase under typical atmospheric conditions. Previous studies demonstrate that IVOCs may be important SOA precursors both in ambient air and in typical source emissions i.e. gasoline vehicles, diesel vehicles and ship emissions (Huang et al., 2018; Zhao et al., 2016, 2015; Zhao et al., 2014). Recent model studies have shown that adding IVOC emissions into different models will greatly improve the SOA simulation results. For example, Giani et al. (2019) found a considerable OA enhancement in Po Valley (Northern Italy) when applying new S/IVOCs emission estimates and the new volatility distributions into CAMx, in which the improvement in SOA mainly due to the revised IVOC emissions. Huang et al. (2020) found a similar enhancement in SOA simulation for Yangtze River Delta (Southeast China) region when adding IVOC emissions into CAMx. They also show the importance of volatility distribution and emission parameterization for the model simulation. Therefore, understanding and characterizing IVOC emissions, as well as their volatility distributions, is crucial for improving numerical models that aim to predict OA.

85   China is in a high-growth stage with rapidly increasing number of on-road

86   vehicles (~26 fold in 25 years). This growth has created a substantial burden on air

87   quality and human health (Hallquist et al., 2016; Hu et al., 2015). During the past few

88   years, many researchers have studied the gases and particulate matter emissions from

89   Chinese vehicles (Cao et al., 2016; Huang et al., 2015). However, none of these

90   studies have reported data on IVOCs emissions from Chinese gasoline vehicles.

91   Although Zhao et al. (2016) characterized IVOC emission in gasoline vehicles in the

92   United States, the results may not be applicable to China given differences in vehicle

93   technologies, operating conditions, and fuel quality. Therefore, understanding and

94   characterizing the IVOC emissions, as well as their volatility distributions from

95   Chinese vehicle, is of vital importance to understand the contribution of IVOCs to

96   SOA formation in China.

97   In this study, IVOCs emissions were measured from a China V gasoline vehicle

98   equipped with a direct inject (GDI) engine during chassis dynamometer testing. The

99   test matrix considered the influence of fuel type and operating conditions on the total

100   IVOC emission factors, including a newly designed cycle designed to simulate

101   Chinese driving conditions. All of the measurements were performed with the same

102   gasoline vehicle in order to consistently evaluate the effects of these different factors

103   on IVOC emissions. The emission factors (EFs), volatility and chemical speciation of

104   IVOC emissions from different conditions were investigated, and the SOA formation

105   potential were estimated.

106

107   **2 Materials and Methods**

108   **2.1 Testing Vehicle, Fuels and Test Cycles**

109   In this study, all measurements were performed on a vehicle chassis

110   dynamometer (Peng et al., 2017) using an in-use light-duty gasoline direct inject (GDI)

111   engine vehicle meeting the China V standard (similar to Euro 5). Tests were

112   conducted with two fuels: commercial China Standard V gasoline and E10 fuel (10%

113   ethanol by volume). The test cycles included the World-wide harmonized Light duty

114   Test Cycle (WLTC), and the Chinese Light vehicles Test Cycle (CLTC). Furthermore,

typical different acceleration rates were also tested. Detailed description and speed profiles of WLTC and CLTC are in Figure S1 in the supplementary information. The CLTC was specifically designed to simulate the driving patterns in Chinese cities while WLTC referred to the Euro VI standard and adopted as China VI testing protocol. Prior to tests, the tested vehicle was preconditioned with an overnight soak, without evaporative canister purge. Different acceleration rates were selected based on their frequency in both CLTC and WLTC, i.e. 1.2, 3.6 6.0 km/h/s, written as ACR1.2, ACR3.6 and ACR6.0), to investigate the effects of acceleration rates on IVOC emissions. All three acceleration "cycles" last for 600 s with a maximum velocity of 70 km/h. The acceleration driving cycles were set according to the criteria of identical cycle period and maximum velocity, and hence the mean velocity for each acceleration cycle is the same (Figure S2). We also measured IVOC emission factors (EFs) when the test vehicle was idling.

2.2 Sampling and Chemical Analysis

Tailpipe emissions were introduced to a constant volume sampler (CVS) that diluted the exhaust by a factor of 20 to 40. For WLTC and CLTC tests, IVOCs emissions were collected by sampling the diluted exhaust through a quartz filter followed by two tandem Tenax TA filled glass tubes (Gerstel, 6 mm OD, 4.5 mm ID glass tube filled with ~180 mg Tenax TA). Sampling tubes and transfer lines from the CVS were kept at a constant temperature (27 ± 2 ^{o}C). The flow rate for quartz filter was 10.0 L/min, and the flow rate for Tenax tube was set as 0.5 L/min. Dynamic blanks were also collected when the CVS was operated with only dilution air (no exhaust) to estimate the contribution of background organic vapors. Prior to sampling, the quartz filters were preheated to 550 °C in air for 6 h in clean aluminum foil using a muffle furnace to remove contaminations. Tenax tubes were preconditioned by using Tube Conditioner (BCT700, BCT Technology LTD), at 300 °C for 3 h in pure nitrogen with a constant flow rate of 100 mL/min. All samples were sealed after sampling and stored in freezer at -20°C.

Quartz filters and Tenax tubes were analyzed using a gas chromatography/mass

spectrometry (Agilent 6890GC/5975MS) equipped with a capillary column (Agilent HP-5MS, 30 m×0.25 mm) coupled to a thermal desorption system (Gerstel, Baltimore, MD). The detailed method was described by Zhao et al.(2014). Prior to analysis, 5 μl of the internal standards (d10-acenaphthene, d12-chrysene, d4-1,4-dichlorobenzene, d8-naphthalene, d12-perylene, d10-phenanthrene and 7 deuterated n-alkanes) were injected into each adsorbent tube to track the IVOCs recovery.

For each test, particulate matter samples were also collected using independent Teflon and quartz filters. The Teflon filters were weighted using a microbalance (Toledo AX105DR, USA) after equilibration for 24 h in an environmental controlled room (temperature $20 \pm 1^{o}C$, relative humidity $40 \pm 3\%$) (Guo et al., 2010). A punch (1.45 cm^2) from each quartz filter was analyzed for organic carbon (OC) and elemental carbon (EC) via thermal-optical method using Sunset Laboratory-based instrument (NIOSH protocol, TOT) (Guo et al., 2012). VOCs were sampled in SUUMA® polished stainless steel canisters and analyzed using GC-MS with a flame ionization detector. Total hydrocarbon (THC), nitrogen oxide, CO and CO_2 emissions under operation scenarios were measured using a Horiba OBS 2200 portable emission system.

2.3 Quantification of IVOCs

Twenty IVOCs compounds were quantified using authentic standards (Table S1). However, the majority of the IVOCs mass appears as a broad hump of co-eluting hydrocarbons and oxygenated organics. These compounds could not be resolved at the molecular level and were therefore classified as an unresolved complex mixture (UCM), which were grouped based on their volatilities.

The total mass of IVOCs was determined following the method of Zhao et al. (2014) (SI) . In short, the TIC of each sample was divided in to 11 retention time bins corresponding to C_{12}-C_{22} n-alkanes. The total mass in each bin was estimated using the instrument response to the n-alkane in that bin. UCM was determined as the difference between total IVOCs and speciated IVOCs in each bin. UCM was then further classified into unspeciated branched alkanes (b-alkanes) and unspeciated

175   cyclic compounds following the approach of Zhao et al. (2016) (SI). The uncertainty

176   of the IVOCs could be ascribed to both sampling and analysis. The sampling

177   uncertainty was assumed as 10% (Huang et al., 2019). The uncertainty of using

178   n-alkanes as surrogate standards for the total IVOC mass was estimated to be less than

179   6.0% for alkanes and 30.6% for PAHs based on the analysis of a suite of standard

180   compounds (SI). Therefore, combined the above uncertainty, we consider a maximum

181   IVOCs mass uncertainty of 32.2% (SI).

182   Fuel-based IVOC emission factors (EF, mg/kg-fuel) were calculated using the

183   carbon-mass-balance method as following

184    $$\text{EF}_{\text{IVOCs}} = \frac{[\Delta IVOC]}{[\Delta CO_2]} f_c$$

185   where $[\Delta IVOC]$ represents the background-corrected mass concentration of

186   IVOCs, $[\Delta CO_2]$ is the background-corrected CO_2 concentration in the CVS expressed

187   in units of carbon mass and f_c is the measured mass fraction of carbon in the gasoline

188   (0.82).

189

190   **3 Results and Discussion**

191   **3.1 Influence of Fuel, Starting Mode, and Operating Cycles on IVOC Emission**

192   **Factors**

193   Figure 1 depicts IVOC EFs of the tested China V gasoline vehicle and compares

194   them with previous studies. The IVOC EFs ranged from 12.1 to 226.3 mg kg-fuel[-1],

195   with a median value of 83.7 mg kg-fuel[-1]. The median IVOC value was ~3 times

196   higher than that of the US LEV-2 gasoline vehicles (21.9 mg kg-fuel[-1]), and one order

197   of magnitude lower than diesel-fueled non-road construction machinery and a

198   diesel-fueled large cargo vessel (971.1 and 800 mg kg-fuel[-1], respectively) (Qi et al.,

199   2019; Huang et al., 2018).

200   Figure 1 summarizes the influences of fuel type, starting mode, operating cycles

201   and acceleration rates on the total IVOC EFs. Various operating conditions may cause

202   different IVOCs emission and fuel consumption. In order to get a relative reliable

203   comparison, what we show here is all described in IVOCs EFs which consider both

IVOCs mass and the fuel consumption. Among all of the factors, acceleration rate has the largest influence on the IVOC EFs. The fuel consumption at high acceleration rate (6.0 km/h/s) would be higher than that at low acceleration rate (idling). Although not emitted in IVOCs, the high consumption of the fuel would exist as other types of carbon e.g. VOCs and CO_2 which may also have great effects on the atmosphere. Therefore, the usage of IVOCs EFs can moderately balance the effects of the IVOCs emission and fuel consumption and get a comprehensive comparison among different acceleration rates. As the acceleration rate increases, the IVOC EF decreases, with the median IVOC EF of ACR6.0 being one order of magnitude lower than that at idling. Qi et al. (2019) and Zhao et al. (2016) report similar results for non-road construction machinery and on-road diesel vehicles, where idling conditions emitted significantly higher IVOCs than those under higher-speed cycles. They proposed that the higher IVOC EFs at idling were the result of less efficient fuel combustion. An additional factor in these tests may be the efficiency of the catalytic converter varying with operating conditions (i.e. lower efficiency at idle operations).

When using commercial China Standard V gasoline, the median IVOC EF was 1.4 times greater than that using Ethanol gasoline, i.e. E10 (10% ethanol, v/v), with median values of 91.5, and 67.6 mg kg-fuel^{-1}, respectively. The median THC EFs for gasoline and E10 were 485 and 589 mg kg-fuel^{-1}, respectively, showing no significant difference.

As expected, The IVOC EFs for cold-start tests was higher (83.7 mg kg-fuel^{-1}) than those for hot-start tests (58.7 mg kg-fuel^{-1}). This reflects the reduced efficiency of the catalytic converter during cold-start operation. The cold-start to hot-start IVOC emission ratio is about 1.4, which is similar to the previous study (Zhao et al., 2016). The median THC EFs for cold-start and hot-start tests are 556.2 and 507.8 mg kg-fuel^{-1}, respectively. Previous studies also show that cold starts have higher THC EFs than hot start operation, but cold-to-hot ratios can span a wide range due to differences in operating conditions and model years(Jaworski et al., 2018; Drozd et al., 2016). The ratio is generally larger for more modern, heavily controlled vehicles(Saliba et al., 2017; May et al., 2014).

234   The median IVOC EF for CLTC was about 1.7 times of that for WLTC (103.5

235   versus 60.9 mg kg-fuel^{-1}). Similar results were also found for THC emission, with

236   median THC EFs for CLTC and WLTC cycle as 617.3 and 420.3 mg kg-fuel^{-1},

237   respectively. Previous studies also show test cycles influence THC EFs. For example,

238   Suarez-Bertoa et al. (2015) and Marotta et al. (2015) found that the NEDC cycle has

239   higher THC EFs than WLTP or WLTC cycle. One possible explanation for the

240   differences between the CLTC and WLTC IVOC EFs is the differences in acceleration

241   rates. A histogram of acceleration rates of the two cycles (Figure S3) shows that

242   CLTC has frequent low acceleration process compared to WLTC. 76.9% of the CLTC

243   has acceleration rates ranging from -1.5 to 1.5 km/h/s versus 69.6% for the WLTC.

244   The CLTC has no acceleration rate higher than 4 km/h/s, suggesting that the gasoline

245   vehicles frequently drive in congested conditions in China.

246   The results from the acceleration rate cycles suggest that the frequent low

247   acceleration rate in CLTC is responsible for the differences of the IVOC EF between

248   CLTC and WLTC. The effect of acceleration on IVOC EFs is probably especially

249   important in urban areas in China, which frequently have substantial traffic

250   congestion. These results underscore the importance of developing cycles that

251   simulate real-world Chinese driving condition e.g. CLTC, instead of using WLTC or

252   other cycles to get relevant emissions data.

253

254   **3.2 Chemical Speciation of Chinese Vehicle IVOCs and the Relationships**

255   **between Total IVOCs, POA and THC**

256   Figure 2 and S4 compare the chemical composition of IVOC emissions from the

257   tested China V vehicle under different operating conditions. In general, IVOC

258   chemical composition was similar across all the tests. Unspeciated IVOCs (UCM)

259   dominates the total IVOCs mass (85.6 ±4.9%), including 65.2 ±5.2% for unspeciated

260   cyclic compounds and 20.4 ±0.7% for unspeciated *b*-alkanes. *n*-alkanes and speciated

261   aromatics contribute 10.9 ±4.7% and 3.5 ±1.7% of the total IVOC mass, respectively.

262   These results are similar to previous studies. For example, Zhao et al. (2016) found

263   the consistent composition of IVOC emissions across a wide set of vehicles.

264   Since the majority of the IVOC mass appears as UCM, the average mass spectra

265   provide additional insight into its composition. A similar distribution of mass

266   fragments was observed across all tests. Figure 2(b) shows the average IVOC mass

267   spectrum collected during an E10 CLTC test. Mass fragments associated with

268   aliphatic hydrocarbons (m/z 43, 57, 71, 85) are the most abundant followed by those

269   associated with aromatics (m/z 91, 105 and 119 for alkylbenzenes (Pretsch et al.,

270   2013), and m/z 115, 165, 189 for poly aromatic species) (Dall'Osto et al., 2009;

271   Spencer et al., 2006).

272   Figures 2(c) and (d) exhibit the contribution of selected mass fragments in low

273   and high volatility ranges, i.e. B_{12}-B_{16} and B_{17}-B_{22}. Aliphatic fragments are higher than

274   aromatics fragments in both B_{12}-B_{16} and B_{17}-B_{22} bins. Compared to the higher

275   volatility (B_{12}-B_{16}) bins, the ratio of selected aromatic to aliphatic fragments is lower

276   in the lower volatility (B_{17}-B_{22}) bins (0.8 versus 1.7) which suggests different

277   weighting of compounds in different volatility range. Therefore, unspeciated IVOC

278   UCM in B_{12}-B_{16} are predominantly aromatics while B_{17}-B_{22} are more abundant in

279   cyclic alkanes.

280   Figure 3 and S5 shows the volatility distribution of IVOC emissions over the 11

281   retention-time bins (B_{12}-B_{22}). IVOC emissions are more heavily weighted towards the

282   more volatile end of the distribution, with more than 50% of the emissions in B_{12}-B_{14}

283   bins. After B_{14}, the IVOC emission decreases significantly.

284   Although the IVOC EFs varied by an order of magnitude across the set of tests

285   (Figure 1), the volatility distributions of the emissions were largely the same. When

286   the vehicle is fueled by gasoline, the median IVOC fractions in the B_{12}-B_{14} bins are

287   slightly higher than when fueled by E10 (Figure S5a). Cold-start has a higher median

288   percentage of IVOC in B_{12}-B_{14} bins compared to hot-start (Figure S5b). No distinct

289   differences in volatility differences between the CLTC and WLTC (Figure S5c).

290   Compared with idling condition, acceleration cycles have higher median percentage

291   of IVOC in lower volatility bins (B_{17}-B_{22}) (Figure S5d), similar to previous studies (Qi

292   et al., 2019; Cross et al., 2015).The modest variations of volatility distributions of the

293   IVOCs emissions may be due to differences in combustion efficiency and/or catalytic

294 converter efficiency as a function of volatility.

295 Considering the similarity of volatility distribution for different conditions and
296 the importance of the volatility distribution in model input for SOA simulation, figure
297 S6 and Table S3 present the volatility distribution of SVOC and IVOC emissions from
298 the tested China V gasoline vehicle, using effective saturation concentration (C*) as
299 classification: IVOCs (C*=300-3 $\times$ 10^6 μg m^{-3}), SVOCs (C*=0.3-300 μg·m^{-3}).
300 IVOCs are the dominant part of the low volatility organics (IVOCs+SVOCs), with a
301 median contribution of ~95%.

302 Previous studies have used different scaling approaches to estimate IVOC
303 emissions using other primary emission data, e.g. POA, NMHC (Murphy et al., 2017;
304 Woody et al., 2016; Koo et al., 2014). However, these ratios depend on fuel, engine
305 technology and operating conditions (Lu et al., 2018).Therefore, it is important to
306 quantify the relationships between IVOCs and other pollutants using data collected
307 from Chinese vehicles. Our results show that the IVOC-to-THC ratio does depend on
308 fuel composition. The average IVOC-to-THC ratios for gasoline-fueled and
309 E10-fueled gasoline vehicle are 0.07 $\pm$ 0.01(R^2 = 0.87) and 0.11 $\pm$ 0.02 (R^2 = 0.78),
310 respectively (Figure S7). The IVOC-to-THC ratios in this study are higher than US
311 vehicles (IVOC-to-NMHC of 0.04) (Zhao et al., 2016) but much lower than diesel
312 fueled vehicles (IVOC-to-THC of 0.67) (Huang et al., 2018). The IVOC-to-POA ratio
313 was 5.12 $\pm$ 1.30 across all tests, but with only modest correlation (R^2 of 0.66 for
314 gasoline-fueled vehicle and 0.43 for E10-fueled vehicle). This ratio is similar to US
315 data for gasoline vehicles. The correlation of IVOC to THC or POA in our dataset is
316 lower than that of the on-road gasoline and diesel vehicles measured in US. This may
317 be caused to the US data are from a large fleet of vehicles while our data is from a
318 single vehicle operated over a range of conditions

319

3.3 High Emission Factors and Distinct Volatility Distributions of IVOCs from Chinese Gasoline Vehicles

322 Figure 4 presents PM, NO_x, THC and IVOC EFs of the tested gasoline vehicle
323 (China V) and compares them to US vehicles tested by Zhao et al. (Zhao et al., 2016;

324   May et al., 2014) For this comparison, we combined all of the CLTC and WLTC data

325   together. The US vehicles are grouped by model year where pre-LEV refers to

326   vehicles manufactured prior to 1994, LEV-1 represents vehicles manufactured

327   between 1994-2003, and LEV-2 indicates vehicles manufactured between 2004-2012.

328   The emissions of NO_x and THC from tested vehicle are comparable with those

329   from the newer (LEV-2) US vehicles tested by May et al. (Zhao et al., 2016; May et

330   al., 2014). However, PM EF (44.8 mg kg-fuel^{-1}) of the tested vehicle is higher than

331   the LEV-2 vehicles tested (17.0 mg kg-fuel^{-1}). It is comparable to a pre-LEV vehicle

332   (61.0 mg kg-fuel^{-1}). In addition, we compared our results with that from European

333   vehicles, and found that the NO_x and THC EFs for the tested vehicle were lower than

334   Euro 5 gasoline vehicle, while the PM EF was higher (Fontaras et al., 2014). This

335   suggests that compared with US and European vehicles, the stringent emission

336   implemented by Chinese government have been effective at controlling NO_x and THC,

337   but might be inefficient to PM emissions. For past 30 years, Chinese government has

338   adopted a series of emission control policies and measures for light-duty vehicles,

339   including implementation of emission standards for new vehicles promotion of

340   sustainable transportation and alternative fuel vehicles, and traffic management

341   programs (Wu et al., 2017; Zhang et al., 2014). Wu et al. (2017) summarizes the

342   implementation of the vehicle control policies in China, which shows the control for

343   the vehicular pollutants is becoming stricter step by step. For example, the NO_x

344   emission standard changed from 0.15 g km^{-1} to 0.035 g km^{-1} while the standard

345   changed from China III to China VI. Different from NO_x and THC which has been

346   controlled since China III, only when in 2017, China V standard first introduced the

347   control of PM into the emission control scope. Yang et al. (2020)investigated the

348   effects of gasoline upgrade policy on migrating the PM pollution in China and found

349   that there's no much space for significantly reducing the PM concentration by simply

350   improving the gasoline quality. Therefore, for PM control, more policies i.e.

351   developing cleaner alternatives to fossil fuels, replacing traditional vehicles with

352   new-energy and building developed public transport system should be done.

353   The IVOC EFs for the tested China V vehicle is between the US Pre-LEV and

354 LEV-1 vehicle. Therefore, Chinese regulations may also appear to be ineffective at
355 controlling IVOC emissions. The IVOC-to-THC ratio measured here (0.07 for
356 gasoline and 0.11 for E10) is higher than US vehicles (0.04), which means that IVOCs
357 contribute a larger fraction of the THC emissions from the China V than from the US
358 vehicles. A detailed comparison of the individual VOC emissions between China V
359 and US LEV-2 vehicles is in SI (Figure S9).

360 UCM accounts for large fraction of IVOCs for both China V and US gasoline
361 vehicles. However, the speciated compounds exhibit different characteristics. The
362 China V exhaust has less speciated IVOC aromatic compounds (3.5%) and more
363 alkanes (10.9%) compared to US exhaust (12.9% and 2.5%, respectively). This is also
364 reflected by the IVOC mass spectrum, where Chinese vehicle exhaust has higher *m/z*
365 43, 57, 71, 85 signals. In addition, the specific aromatics mass fragments were not the
366 same for China V and US IVOC emissions. For example, the dominant aromatics
367 fragments in US gasoline exhaust are *m/z* 128, 119, 105, 133 versus *m/z* 135, 91, 181,
368 189 for China V. (Fig. 2c and d).

369 Figure 3 compares the volatility distribution of the IVOC emissions from the
370 China V and US vehicles. There are significant differences of volatility distribution
371 between China V and US vehicles. Both distributions decrease with the increase of
372 the retention time, but the IVOC volatility distribution of US vehicle exhaust exhibits
373 heavier weight of lower volatility bin, i.e. B_{12} bin compared to the China V vehicle. In
374 US exhaust the B_{12} fraction is more than double of the B_{13}. However, the contributions
375 of B_{12}-B_{14} bin volatility bins are comparable for Chinese vehicle exhaust. US vehicle
376 exhaust has a similar IVOC volatility distribution as the unburned gasoline, indicating
377 that the evaporate of IVOCs from fuel is non neglectable.

378 The differences between the IVOC volatility distribution between the Chinese
379 vehicle exhaust and unburned gasoline were further investigated. The higher emission
380 factor and broader distribution of IVOCs in exhaust from China V compared with US
381 vehicles may be due to differences in fuel composition, operating conditions and
382 engines and after-treatment technology. As the tests of US vehicles were all
383 performed using California commercial fuel, which is, in fact, E10 fuel. Therefore, in

Lu et al. (2018) demonstrated that IVOC emissions depend strongly on fuel composition. In our study, IVOCs contributed ~2.0 wt% (2.1 wt% for gasoline, 1.9 wt% for E10) of the total fuel mass, which is ~60% higher than the California fuel (E10, 1.2 wt%)(Gentner et al., 2012). Therefore, the higher IVOC fractions in China V exhaust (e.g. IVOC-to-THC ratio of 0.07 and 0.11 versus 0.04 in US exhaust) may lead to higher amounts of IVOCs in China V gasoline. When considering volatility distribution, Zhao et al. (2016) and Lu et al. (2018) reported similar distributions of IVOC between gasoline vehicle exhaust and unburned fuel, which demonstrates the significant influence of unburned fuel on exhaust volatility distribution. As a result, in Figure 3, we use US gasoline vehicle exhaust to both represent the exhaust and the unburned (E10) fuel and compare the Chinese E10 fuel with US fuel to get a comparative study. However, the volatlity distribution of the China V gasoline vehicle exhaust are different from that of the unburned fuel (Figure 3). The difference might be related to the operating conditions and engine-aftertreatment system.

Although operating conditions strongly influence the total IVOC EFs (Figure 1), Figure 3 indicates the volatility distribution of the IVOCs emissions were largely consistent across the set of test conditions. Therefore, operating conditions cannot explain the difference in the IVOC volatility distribution between the China V vehicle, unburned gasoline, and the US vehicles.

The engine-aftertreatment system also influences IVOC emissions (Drozd et al., 2019; Alam et al., 2019; Zhao et al., 2018; Saliba et al., 2017). In order to investigate the efficiency of after-treatment system, we normalized the IVOC distributions of the fuel and exhaust to the sum of C_8-C_{10} n-alkanes. It is believed that the C_8-C_{10} n-alkanes can serve as the indicators for VOCs in fuel (Lu et al. 2018). For both US and the China V vehicles, IVOCs are enriched in the exhaust relative to the fuel. However, the enrichment factor is much smaller in Chinese exhaust with a median value of 4.0 than that for US vehicles (median value = 8.5) (Lu et al., 2018). The enrichment factor also varies with different compounds, with the enrichment factors

413 of *n*-alkanes (9.3)＞*b*-alkanes (6.6)＞unspeciated cyclic ompounds (3.1)＞aromatics

414 (0.4). These results are consistent with previous studies stating that the aftertreatment

415 devices have different removal efficiency towards different compounds (Ma et al.,

416 2019; Hasan et al., 2018; Hasan et al., 2016; Alam and Harrison, 2016). Our results

417 suggest that the Chinese three-way catalytic converter has compound dependent

418 efficiency (better removal of aromatics compared to alkanes) which might explain the

419 difference in compound composition between Chinese and US vehicle exhaust.

420 Furthermore, Fig. S10 shows that the catalytic converter has different removal

421 capacity towards different volatility bins, in which B_{14-16} works much worse compared

422 to other volatility bins i.e. B_{12}. Consequently, the SOA formation would be relatively

423 high. In sum, the compound dependent capacity and lower B_{14}-B_{16} removal efficiency

424 of Chinese TWC is responsible for the volatility distribution differences between

425 China V and US vehicles shown in Figure 3.

426   After considering all the factors above, we can draw the conclusion that fuel type,

427 starting mode and operating conditions can all affect the IVOCs EFs. The only factor

428 that impacts the volatility distribution is engine-aftertreament system.

3.4 Estimation of SOA Production from Chinses Vehicle Emission

430   With the measured IVOC and VOC emissions, we estimated the SOA formation

431 potential by using the yield method as following (Yuan et al., 2013):

432      $$\Delta SOA/\Delta CO = \sum ER_{[HC]_i} \times \left(1 - e^{-(k_{OH,i}-k_{CO}) \times [OH] \times \Delta t}\right) \times Y_i$$

433   In which, $ER_{[HC]_i}$ is the emission ratio of SOA precursor i (mg kg-fuel^{-1}); $k_{OH,i}$

434 is the OH reaction rate constant of precursor i at 298K (cm^3 molecules^{-1} s^{-1}); k_{CO} is

435 the OH reaction constant of CO at 298 K (2.4×10^{-13} cm^3 molecules^{-1} s^{-1}); [OH] is the

436 OH mixing ratio, which is assumed to be 1.5×10^6 molecules cm^3 (Lu et al., 2019); Δt

437 is photochemical age (h); and Y_i is the SOA yield determined from chamber studies.

438 Previous studies have shown that the SOA yield of individual hydrocarbon can be

439 influenced by NO_x level, due to the competition reactions among RO_2 radicals, NO

440 and HO_2 radicals. Usually SOA yields under low NO_x condition are independent on

441 the OA loading. However, under high NO_x condition, SOA yields highly depend on

OA mass concentration, which can be described using two-product or multi-products model (Presto et al., 2010; Chan et al., 2009; Ng et al., 2007). In this study, we estimated SOA formation under low and high NO_x conditions with OA concentration of 10, 20, 80 $\mu g \cdot m^{-3}$ to represent the influence of NO_x level and OA loading on SOA formation.

In this estimation, we include speciated C_6-C_9 single ring aromatics (SRAs) as typical VOCs for SOA precursors, and the corresponding k_{OH} and SOA yields are extrapolated according to two-product relationship from chamber studies (see SI) (Ng et al., 2007). The SOA yields under low and high NO_x condition, and the OH reaction rates of speciated IVOCs and SRAs are from the previous studies (see SI) (Presto et al., 2010; Lim and Ziemann, 2009; Chan et al., 2009). In brief, surrogate species were used to represent the unspeciated *b*-alkanes and cyclic compounds in each of the volatility bins.

Figure 5 shows the POA emission and estimated SOA production under different operating conditions and NO_x level after 48 h of photo-oxidation. The estimated SOA/POA ratio is between 4.0 to 5.0 under low NO_x condition, and the SOA-to-POA ratios ranged from 1.8-2.2 to 3.8-4.4 when the OA loading increased from 10 $\mu g \cdot m^{-3}$ to 80 $\mu g \cdot m^{-3}$ under high NO_x condition. The OA enhancement under low NO_x condition is similar to that under high NO_x condition with the OA loading of 80 $\mu g \cdot m^{-3}$. Considering the high POA concentration and SOA formation capacity of Chinese gasoline vehicles, the SOA/POA ratios at 80 $\mu g \cdot m^{-3}$ are considered as a lower estimation. Compared with OA enhancement from US studies (~3.6) (Zhao et al., 2016), our results showed higher SOA formation potential both under low and high NO_x conditions for Chinese gasoline vehicles.

Scenario-based analysis shows similar tendency of SOA formation potential at different OA loading under low and high NO_x condition. Though the POA emission for gasoline-fueled vehicle was higher than that fueled by E10, comparable SOA formation is estimated using gasoline and E10 as fuel. That means, the OA enhancement factor for E10 is higher than that of gasoline. This suggests that although the ongoing policy of ethanol gasoline will not exacerbate the POA emission

472   in China, the SOA formation of E10 could not be neglected due to its high SOA

473   enhancement capacity. Therefore, more research should be done to evaluate the

474   effectiveness of using E10 as surrogate to reduce the air pollution in China.

475   Cold-start operation has higher SOA potential with higher OA enhancement

476   factor than hot-start, due to the higher precursors EFs caused by the reduced catalytic

477   converter effectiveness below its light off temperature (Drozd et al., 2019). The IVOC

478   EFs, the estimated SOA production and SOA/POA of CLTC are all higher than those

479   of WLTC, which further demonstrates the higher SOA formation potential of Chinese

480   gasoline vehicles under typical driving conditions in China.

481   Figure S11 presents the contribution of different classes of precursors on the

482   SOA production after 48 h of photo-oxidation under different OA loading and NO_x

483   condition. The relative contributions of different chemical classes were similar across

484   the different conditions, with the largest contribution from unspeciated cyclic IVOCs.

485   This is different from the US gasoline vehicle SOA (Zhao et al., 2016) in which single

486   ring aromatics contributes the most.

487

3.5 Establishing the Estimation Method of SOA formation from Chinese

Gasoline Vehicles

490   In this section, we tried to establish parameterization methods to provide simple

491   estimations of gasoline vehicle SOA based on our measurements of VOCs and

492   IVOCs.

493   Figure S12 shows the average predicted SOA-to-POA ratio as the function of

494   photo-oxidation time under different OA loading and NO_x conditions. In general,

495   SOA exceeds POA after first a few hours of oxidation, and then levels off after 30 h.

496   The SOA/POA ratio is influenced by OA concentration, NO_x level and the

497   photochemical age (OH exposure). At a certain OA loading and OH exposure,

498   SOA/POA ratio can be estimated, and then be used to quantify the contributions of

499   gasoline vehicle SOA to the ambient OA. Therefore, we parameterized the SOA/POA

500   variation under different OA and NO_x condition using three-parameter-based

501   logarithm equation, i.e. $y = a - b \times \ln(t+c)$, in which t represents the equivalent

502 photochemical age (assume that the OH concentration is 1.5×10^6 molecules cm^3) and

503 a, b, c can be described using three-parameter logarithm equation y=m-n×ln([OA

504 concentration]+p). Table 1 shows the parameterization results of compounds-based

505 SOA/POA variation under the different OA and NO$_x$ condition. The fits quality could

506 be found in Figure S13.

507 Table 1 Coefficient of parameterization between SOA/POA and photochemical age

SOA/POA	Low NO$_x$ condition	High NO$_x$ condition		
		m	n	p
a	-0.62	0.46	0.22	9.8
b	-1.34	0.27	0.33	2.58
c	0.58	0.13	-0.09	3.35
Unspeciated cyclic compounds				
a	-0.15	0.26	0.09	21.76
b	-0.72	0.086	0.18	0.46
c	0.11	-0.278	-0.083	24.42
Unspeciated b-alkanes				
a	-0.11	0.47	0.111	87.54
b	-0.17	0.15	0.070	12.36
c	0.84	-0.17	-0.21	41.97
aromatics				
a	-0.03	-0.023	-0.0098	40.52
b	-0.03	0.012	0.007	17.27
c	-1.00	-1.02	-0.021	-10.00
n-alkanes				
a	-0.05	0.0067	0.013	-2.38
b	-0.11	0.019	0.030	-0.52
c	0.48	0.15	-0.058	29.18
Single ring aromatics				
a	-0.51	0.28	0.17	5.47
b	-0.35	0.03	0.059	-2.29
c	3.92	2.80	-1.29	10.84

The above photochemical-based parameterization method provides a conservative way to quantify the evolution of SOA from Chinese gasoline vehicle VOCs and IVOCs oxidation. However, there are still some uncertainties which may lead to discrepancies between predicted and measured SOA. In general, positive or negative artifacts of quartz filters, *n*-alkane equivalent method in estimating the IVOCs concentration, uncertainty in SOA yield, surrogate method to substitute SOA yield and k_{OH} for UCM and lack of semi-volatile organic compounds will exert influence on the SOA prediction.

4 Atmospheric Implications

We measured the VOCs, IVOCs and POA emitted from a China V light duty gasoline vehicle across a wide range of operating conditions. Compared with US LEV-2 gasoline vehicles, the China V vehicle emits three times more IVOCs. Besides, the IVOC emissions from the China V vehicle have a much broader volatility distribution than that from US vehicles. These characteristics imply that IVOCs could act more important SOA precursors in China than those in the US. For Chinese gasoline vehicles, although the magnitude of the emission of IVOCs and VOCs can vary, their relative contribution to SOA production is similar across the set of operating conditions examined here due to the similar volatility distributions. As a result, the key to control SOA formation of gasoline vehicles is to reduce the total IVOC EFs by upgrading of emissions controls. In addition, reducing congestion and other low speed operating modes would also be effective at reducing emissions (Figure 1 and 5).

Based on our results, we roughly estimate the vehicle IVOC emissions in China. Till the end of 2018, the total vehicle population in China reached 0.327 billion, with automobiles contributing 61% (0.24 billion). Of all the automobiles, gasoline-fueled car took the dominant (88.1%). The HC emission of gasoline vehicles in China was 0.23 Mt, accounting for more than 70% of the total vehicle emissions. Using an IVOC/THC ratio of 0.09 that is obtained in our work, we estimate that the vehicle IVOC emissions in China are 0.03 Mt (30 Gg), in which 20 Gg is attributed to

538 gasoline vehicles. One should note that this estimation is a conservative value, since

539 we consider all vehicles as gasoline vehicles, and all of them meet the China V

540 standard. According to the statistics from the Ministry of Ecology and Environment,

541 only 30.9% of the vehicles in 2018 meet the standards of China V. Indeed, higher

542 percentage of pre-China V e.g. China I-IV standard cars will cause more IVOCs

543 emission. In addition,   the IVOC/NMHC ratio of diesel vehicles could be much

544 higher than that of the gasoline vehicles (Zhao et al., 2016, 2015). This may also lead

545 to an underestimation.

546 Our results show that using a Chinese real-world test protocol CLTC will result

547 in substantially higher IVOC emissions compared with WLTC which might have

548 close relationship with frequent idling and low acceleration condition. Therefore,

549 when driving at typical Chinese condition where traffic congestion frequently occur,

550 the IVOCs emission from Chinese gasoline vehicles would be much higher than the

551 current limited emission inventory. Our results indicate simply controlling the THC,

552 NO_x and primary PM emissions may be insufficient in the aspect of controlling

553 particle pollution. Reducing IVOC emissions should also be taken into consideration

554 due to their high contribution to SOA formation, which is more important than

555 primary organic aerosol. Suggested controlling ways include upgrading the fuel

556 quality and engine-after treatment system, and reducing the traffic congestion.

557 Though we have discussed the influences of different operating conditions on

558 IVOC emissions and SOA formation for the tested China V gasoline vehicle, due to

559 the singular vehicle tests of our study, more research i.e. vehicles meeting different

560 emission standards, different engines should be performed both to testify the accuracy

561 of our research and to get a full understanding of the IVOC emission inventory for

562 Chinese gasoline vehicles. Furthermore, advanced measurement techniques e.g. GC×

563 GC-MS and chemical ionization mass spectrometry (CIMS) should be used to obtain

564 a comprehensive molecular-level picture of the total organics so as to reduce the

565 uncertainties associated with the measurements and models.

566

567 *Data availability*

The data used in this publication are available on https://doi.org/10.5281/zenodo.4072847, and they can be accessed by request to the corresponding author (songguo@pku.edu.cn) of Peking University. The IVOCs emissions from US vehicles used in this study can be accessed via https://pubs.acs.org/doi/abs/10.1021/acs.est.5b06247 (Zhao et al., 2016) and https://acp.copernicus.org/articles/18/17637/2018/ (Lu et al, 2018). The primary emissions and fuel compositions from US vehicles used in this study can be accessed via https://www.sciencedirect.com/science/article/pii/S1352231014000715 (May et al., 2014).

Competing interests

The authors declare that they have no conflict of interest.

Author contributions

SG, RZ and HW designed the study. RZ and KS collected the samples. RZ and QL analyzed the samples and processed the data. RZ wrote the paper, with contributions from all the coauthors.

599

References

Alam, M. S., and Harrison, R. M.: Recent advances in the application of 2-dimensional gas chromatography with soft and hard ionisation time-of-flight mass spectrometry in environmental analysis, Chemical Science, 7, 3968-3977, 10.1039/c6sc00465b, 2016.

Alam, M. S., Zeraati-Rezaei, S., Xu, H., and Harrison, R. M.: Characterization of Gas and Particulate Phase Organic Emissions (C9–C37) from a Diesel Engine and the Effect of Abatement Devices, Environmental science & technology, 53, 11345-11352, 2019.

Cao, X., Yao, Z., Shen, X., Ye, Y., and Jiang, X.: On-road emission characteristics of VOCs from light-duty gasoline vehicles in Beijing, China, Atmospheric Environment, 124, 146-155, https://doi.org/10.1016/j.atmosenv.2015.06.019, 2016.

Chan, A. W. H., Kautzman, K. E., Chhabra, P. S., Surratt, J. D., Chan, M. N., Crounse, J. D., Kuerten, A., Wennberg, P. O., Flagan, R. C., and Seinfeld, J. H.: Secondary organic aerosol formation from photooxidation of naphthalene and alkylnaphthalenes: implications for oxidation of intermediate volatility organic compounds (IVOCs), Atmospheric Chemistry and Physics, 9, 3049-3060, 10.5194/acp-9-3049-2009, 2009.

Cross, E. S., Sappok, A. G., Wong, V. W., and Kroll, J. H.: Load-Dependent Emission Factors and Chemical Characteristics of IVOCs from a Medium-Duty Diesel Engine, Environmental Science & Technology, 49, 13483-13491, 10.1021/acs.est.5b03954, 2015.

Dall'Osto, M., Harrison, R., Coe, H., and Williams, P.: Real-time secondary aerosol formation during a fog event in London, Atmospheric Chemistry and Physics, 9, 2459-2469, 2009.

Donahue, N. M., Robinson, A. L., Stanier, C. O., and Pandis, S. N.: Coupled partitioning, dilution, and chemical aging of semivolatile organics, Environmental Science & Technology, 40, 2635-2643, 10.1021/es052297c, 2006.

Drozd, G. T., Zhao, Y., Saliba, G., Frodin, B., Maddox, C., Weber, R. J., Chang, M. C. O., Maldonado, H., Sardar, S., Robinson, A. L., and Goldstein, A. H.: Time Resolved Measurements of Speciated Tailpipe Emissions from Motor Vehicles: Trends with Emission Control Technology, Cold Start Effects, and Speciation, Environmental Science & Technology, 50, 13592-13599, 10.1021/acs.est.6b04513, 2016.

Drozd, G. T., Zhao, Y., Saliba, G., Frodin, B., Maddox, C., Chang, M. C. O., Maldonado, H., Sardar, S., Weber, R. J., Robinson, A. L., and Goldstein, A. H.: Detailed speciation of intermediate volatility and semivolatile organic compound emissions from gasoline vehicles: effects of cold starts and implications for secondary organic aerosol formation, Environmental Science & Technology, 53, 1706-1714, 10.1021/acs.est.8b05600, 2019.

Fontaras, G., Franco, V., Dilara, P., Martini, G., and Manfredi, U.: Development and review of Euro 5 passenger car emission factors based on experimental results over various driving cycles, Science of The Total Environment, 468-469, 1034-1042, https://doi.org/10.1016/j.scitotenv.2013.09.043, 2014.

Gentner, D. R., Isaacman, G., Worton, D. R., Chan, A. W. H., Dallmann, T. R., Davis, L., Liu, S., Day, D. A., Russell, L. M., Wilson, K. R., Weber, R., Guha, A., Harley, R. A., and Goldstein, A. H.: Elucidating secondary organic aerosol from diesel and gasoline vehicles through detailed characterization of organic carbon emissions, Proceedings of the National Academy of Sciences of the United States of America, 109, 18318-18323, 2012.

Giani, P., Balzarini, A., Pirovano, G., Gilardoni, S., Paglione, M., Colombi, C., Gianelle, V. L., Belis, C. A., Poluzzi, V., and Lonati, G.: Influence of semi- and intermediate-volatile organic compounds

(S/IVOC) parameterizations, volatility distributions and aging schemes on organic aerosol modelling in winter conditions, Atmospheric Environment, 213, 11-24, 10.1016/j.atmosenv.2019.05.061, 2019.

Guo, S., Hu, M., Wang, Z. B., Slanina, J., and Zhao, Y. L.: Size-resolved aerosol water-soluble ionic compositions in the summer of Beijing: implication of regional secondary formation, Atmospheric Chemistry and Physics, 10, 947-959, 2010.

Guo, S., Hu, M., Guo, Q., Zhang, X., Schauer, J. J., and Zhang, R.: Quantitative evaluation of emission controls on primary and secondary organic aerosol sources during Beijing 2008 Olympics, Atmospheric Chemistry and Physics, 13, 8303-8314, 2012.

Guo, S., Hu, M., Shang, D. J., Guo, Q. F., and Hu, W. W.: Research on Secondary Organic Aerosols Basing on Field Measurement, Acta Chimica Sinica, 72, 145-157, 10.6023/a13111169, 2014a.

Guo, S., Hu, M., Zamora, M. L., Peng, J., Shang, D., Zheng, J., Du, Z., Wu, Z., Shao, M., Zeng, L., Molina, M. J., and Zhang, R.: Elucidating severe urban haze formation in China, Proceedings of the National Academy of Sciences of the United States of America, 111, 17373-17378, 10.1073/pnas.1419604111, 2014b.

Hallquist, M., Wenger, J. C., Baltensperger, U., Rudich, Y., Simpson, D., Claeys, M., Dommen, J., Donahue, N. M., George, C., Goldstein, A. H., Hamilton, J. F., Herrmann, H., Hoffmann, T., Iinuma, Y., Jang, M., Jenkin, M. E., Jimenez, J. L., Kiendler-Scharr, A., Maenhaut, W., McFiggans, G., Mentel, T. F., Monod, A., Prevot, A. S. H., Seinfeld, J. H., Surratt, J. D., Szmigielski, R., and Wildt, J.: The formation, properties and impact of secondary organic aerosol: current and emerging issues, Atmospheric Chemistry and Physics, 9, 5155-5236, 2009.

Hallquist, M., Munthe, J., Hu, M., Wang, T., Chan, C. K., Gao, J., Boman, J., Guo, S., Hallquist, A. M., and Mellqvist, J.: Photochemical smog in China: scientific challenges and implications for air-quality policies, National Science Review, 3, 401-403, 2016.

Hasan, A. O., Abu-jrai, A., Al-Muhtaseb, A. a. H., Tsolakis, A., and Xu, H.: Formaldehyde, acetaldehyde and other aldehyde emissions from HCCI/SI gasoline engine equipped with prototype catalyst, Fuel, 175, 249-256, https://doi.org/10.1016/j.fuel.2016.02.005, 2016.

Hasan, A. O., Elghawi, U. M., Al-Muhtaseb, A. a. H., Abu-jrai, A., Al-Rawashdeh, H., and Tsolakis, A.: Influence of composite after-treatment catalyst on particle-bound polycyclic aromatic hydrocarbons–vapor-phase emitted from modern advanced GDI engines, Fuel, 222, 424-433, https://doi.org/10.1016/j.fuel.2018.02.114, 2018.

Hu, M., Guo, S., Peng, J., and Wu, Z.: Insight into characteristics and sources of PM2.5 in the Beijing–Tianjin–Hebei region, China, National Science Review, 2, 257-258, 2015.

Huang, C., Wang, H., Li, L., Wang, Q., Lu, Q., De Gouw, J., Zhou, M., Jing, S., Lu, J., and Chen, C.: VOC species and emission inventory from vehicles and their SOA formation potentials estimation in Shanghai, China, Atmospheric Chemistry and Physics, 15, 11081-11096, 2015.

Huang, C., Hu, Q., Li, Y., Tian, J., Ma, Y., Zhao, Y., Feng, J., An, J., Qiao, L., Wang, H., Jing, S. a., Huang, D., Lou, S., Zhou, M., Zhu, S., Tao, S., and Li, L.: Intermediate Volatility Organic Compound Emissions from a Large Cargo Vessel Operated under Real-world Conditions, Environmental Science & Technology, 52, 12934-12942, 10.1021/acs.est.8b04418, 2018.

Huang, G., Liu, Y., Shao, M., Li, Y., Chen, Q., Zheng, Y., Wu, Z., Liu, Y., Wu, Y., and Hu, M.: Potentially Important Contribution of Gas-Phase Oxidation of Naphthalene and Methylnaphthalene to Secondary Organic Aerosol during Haze Events in Beijing, Environmental Science & Technology, 53, 1235-1244, 2019.

Huang, L., Wang, Q., Wang, Y., Emery, C., Zhu, A., Zhu, Y., Yin, S., Yarwood, G., Zhang, K., and Li,

L.: Simulation of secondary organic aerosol over the Yangtze River Delta region: The impacts from the emissions of intermediate volatility organic compounds and the SOA modeling framework, Atmospheric Environment, 118079, 10.1016/j.atmosenv.2020.118079, 2020.

Jaworski, A., Kuszewski, H., Ustrzycki, A., Balawender, K., Lejda, K., and Woś, P.: Analysis of the repeatability of the exhaust pollutants emission research results for cold and hot starts under controlled driving cycle conditions, Environmental Science and Pollution Research, 25, 17862-17877, 10.1007/s11356-018-1983-5, 2018.

Kanakidou, M., Seinfeld, J., Pandis, S., Barnes, I., Dentener, F., Facchini, M., Dingenen, R. V., Ervens, B., Nenes, A., and Nielsen, C.: Organic aerosol and global climate modelling: a review, Atmospheric Chemistry and Physics, 5, 1053-1123, 2005.

Koo, B., Knipping, E., and Yarwood, G.: 1.5-Dimensional volatility basis set approach for modeling organic aerosol in CAMx and CMAQ, Atmospheric Environment, 95, 158-164, https://doi.org/10.1016/j.atmosenv.2014.06.031, 2014.

Lim, Y. B., and Ziemann, P. J.: Effects of molecular structure on aerosol yields from OH radical-initiated reactions of linear, branched, and cyclic alkanes in the presence of NO x, Environmental science & technology, 43, 2328-2334, 2009.

Lu, K., Guo, S., Tan, Z., Wang, H., Shang, D., Liu, Y., Li, X., Wu, Z., Hu, M., and Zhang, Y.: Exploring atmospheric free-radical chemistry in China: the self-cleansing capacity and the formation of secondary air pollution, National Science Review, 6, 579-594, 2019.

Lu, Q., Zhao, Y., and Robinson, A. L.: Comprehensive organic emission profiles for gasoline, diesel, and gas-turbine engines including intermediate and semi-volatile organic compound emissions, Atmospheric Chemistry and Physics, 18, 17637-17654, 2018.

Ma, R., He, X., Zheng, Y., Zhou, B., Lu, S., and Wu, Y.: Real-world driving cycles and energy consumption informed by large-sized vehicle trajectory data, Journal of Cleaner Production, 223, 564-574, https://doi.org/10.1016/j.jclepro.2019.03.002, 2019.

Marotta, A., Pavlovic, J., Ciuffo, B., Serra, S., and Fontaras, G.: Gaseous Emissions from Light-Duty Vehicles: Moving from NEDC to the New WLTP Test Procedure, Environmental Science & Technology, 49, 8315-8322, 10.1021/acs.est.5b01364, 2015.

May, A. A., Nguyen, N. T., Presto, A. A., Gordon, T. D., Lipsky, E. M., Karve, M., Gutierrez, A., Robertson, W. H., Zhang, M., Brandow, C., Chang, O., Chen, S. Y., Cicero-Fernandez, P., Dinkins, L., Fuentes, M., Huang, S. M., Ling, R., Long, J., Maddox, C., Massetti, J., McCauley, E., Miguel, A., Na, K., Ong, R., Pang, Y. B., Rieger, P., Sax, T., Truong, T., Vo, T., Chattopadhyay, S., Maldonado, H., Maricq, M. M., and Robinson, A. L.: Gas- and particle-phase primary emissions from in-use, on-road gasoline and diesel vehicles, Atmospheric Environment, 88, 247-260, 2014.

Murphy, B. N., Woody, M. C., Jimenez, J. L., Carlton, A. M. G., and Pye, H. O. T.: Semivolatile POA and parameterized total combustion SOA in CMAQv5.2: impacts on source strength and partitioning, Atmospheric Chemistry & Physics, 17, 11107-11133, 2017.

Ng, N., Kroll, J., Chan, A., Chhabra, P., Flagan, R., and Seinfeld, J.: Secondary organic aerosol formation from m-xylene, toluene, and benzene, Atmospheric Chemistry and Physics, 7, 3909-3922, 2007.

Peng, J. F., Hu, M., Du, Z. F., Wang, Y. H., Zheng, J., Zhang, W. B., Yang, Y. D., Qin, Y. H., Zheng, R., Xiao, Y., Wu, Y. S., Lu, S. H., Wu, Z. J., Guo, S., Mao, H. J., and Shuai, S. J.: Gasoline aromatics: a critical determinant of urban secondary organic aerosol formation, Atmospheric Chemistry and Physics, 17, 10743-10752, 10.5194/acp-17-10743-2017, 2017.

731 Presto, A. A., Miracolo, M. A., Donahue, N. M., and Robinson, A. L.: Secondary organic aerosol
732 formation from high-NO(x) photo-oxidation of low volatility precursors: n-alkanes, Environmental
733 Science & Technology, 44, 2029-2034, 2010.

734 Pretsch, E., Clerc, T., Seibl, J., and Simon, W.: Tables of spectral data for structure determination of
735 organic compounds, Springer Science & Business Media, 2013.

736 Qi, L., Liu, H., Shen, X. e., Fu, M., Huang, F., Man, H., Deng, F., Shaikh, A. A., Wang, X., Dong, R.,
737 Song, C., and He, K.: Intermediate-Volatility Organic Compound Emissions from Nonroad
738 Construction Machinery under Different Operation Modes, Environmental Science & Technology, 53,
739 13832-13840, 10.1021/acs.est.9b01316, 2019.

740 Robinson, A. L., Donahue, N. M., Shrivastava, M. K., Weitkamp, E. A., Sage, A. M., Grieshop, A. P.,
741 Lane, T. E., Pierce, J. R., and Pandis, S. N.: Rethinking Organic Aerosols: Semivolatile Emissions and
742 Photochemical Aging, Science, 315, 1259-1262, 2007.

743 Saliba, G., Saleh, R., Zhao, Y., Presto, A. A., Larnbe, A. T., Frodin, B., Sardar, S., Maldonado, H.,
744 Maddox, C., May, A. A., Drozd, G. T., Goldstein, A. H., Russell, L. M., Hagen, F., and Robinson, A. L.:
745 Comparison of Gasoline Direct-Injection (GDI) and Port Fuel Injection (PFI) Vehicle Emissions:
746 Emission Certification Standards, Cold-Start, Secondary Organic Aerosol Formation Potential, and
747 Potential Climate Impacts, Environmental Science & Technology, 51, 6542-6552,
748 10.1021/acs.est.6b06509, 2017.

749 Spencer, M. T., Shields, L. G., Sodeman, D. A., Toner, S. M., and Prather, K. A.: Comparison of oil and
750 fuel particle chemical signatures with particle emissions from heavy and light duty vehicles,
751 Atmospheric Environment, 40, 5224-5235, 2006.

752 Suarez-Bertoa, R., Zardini, A. A., Keuken, H., and Astorga, C.: Impact of ethanol containing gasoline
753 blends on emissions from a flex-fuel vehicle tested over the Worldwide Harmonized Light duty Test
754 Cycle (WLTC), Fuel, 143, 173-182, https://doi.org/10.1016/j.fuel.2014.10.076, 2015.

755 Tang, R., Wu, Z., Li, X., Wang, Y., Shang, D., Xiao, Y., Li, M., Zeng, L., Wu, Z., Hallquist, M., Hu, M.,
756 and Guo, S.: Primary and secondary organic aerosols in summer 2016 in Beijing, Atmos. Chem. Phys.,
757 18, 4055-4068, 10.5194/acp-18-4055-2018, 2018.

758 Tang, R., Wang, H., Liu, Y., and Guo, S.: Constituents of Atmospheric Semi-Volatile and Intermediate
759 Volatility Organic Compounds and Their Contribution to Organic Aerosol, PROGRESS IN
760 CHEMISTRY, 31, 180-190, 2019.

761 Woody, M. C., Wong, H. W., West, J. J., and Arunachalam, S.: Multiscale predictions of
762 aviation-attributable PM2.5 for US airports modeled using CMAQ with plume-in-grid and an
763 aircraft-specific 1-D emission model, Atmospheric Environment, 147, 384-394,
764 10.1016/j.atmosenv.2016.10.016, 2016.

765 Wu, Y., Zhang, S., Hao, J., Liu, H., Wu, X., Hu, J., Walsh, M. P., Wallington, T. J., Zhang, K. M., and
766 Stevanovic, S.: On-road vehicle emissions and their control in China: A review and outlook, Science of
767 The Total Environment, 574, 332-349, 2017.

768 Yang, G., Zhang, Y., and Li, X.: Impact of gasoline upgrade policy on particulate matter pollution in
769 China, Journal of Cleaner Production, 262, 121336, 10.1016/j.jclepro.2020.121336, 2020.

770 Yuan, B., Hu, W. W., Shao, M., Wang, M., Chen, W. T., Lu, S. H., Zeng, L. M., and Hu, M.: VOC
771 emissions, evolutions and contributions to SOA formation at a receptor site in eastern China,
772 Atmospheric Chemistry and Physics, 13, 8815-8832, 10.5194/acp-13-8815-2013, 2013.

773 Zhang, Q., Jimenez, J., Canagaratna, M., Allan, J., Coe, H., Ulbrich, I., Alfarra, M., Takami, A.,
774 Middlebrook, A., and Sun, Y.: Ubiquity and dominance of oxygenated species in organic aerosols in

775 anthropogenically‑influenced Northern Hemisphere midlatitudes, Geophysical Research Letters, 34,
776 2007.

777 Zhang, S., Wu, Y., Wu, X., Li, M., Ge, Y., Liang, B., Xu, Y., Zhou, Y., Liu, H., Fu, L., and Hao, J.:
778 Historic and future trends of vehicle emissions in Beijing, 1998–2020: A policy assessment for the
779 most stringent vehicle emission control program in China, Atmospheric Environment, 89, 216-229,
780 https://doi.org/10.1016/j.atmosenv.2013.12.002, 2014.

781 Zhao, Y., Hennigan, C. J., May, A. A., Tkacik, D. S., de Gouw, J. A., Gilman, J. B., Kuster, W. C.,
782 Borbon, A., and Robinson, A. L.: Intermediate-Volatility Organic Compounds: A Large Source of
783 Secondary Organic Aerosol, Environmental Science & Technology, 48, 13743-13750,
784 10.1021/es5035188, 2014.

785 Zhao, Y., Nguyen, N. T., Presto, A. A., Hennigan, C. J., May, A. A., and Robinson, A. L.: Intermediate
786 Volatility Organic Compound Emissions from On-Road Diesel Vehicles: Chemical Composition,
787 Emission Factors, and Estimated Secondary Organic Aerosol Production, Environmental Science &
788 Technology, 49, 11516-11526, 10.1021/acs.est.3b02841, 2015.

789 Zhao, Y., Nguyen, N. T., Presto, A. A., Hennigan, C. J., May, A. A., and Robinson, A. L.: Intermediate
790 Volatility Organic Compound Emissions from On-Road Gasoline Vehicles and Small Off-Road
791 Gasoline Engines, Environmental Science & Technology, 50, 4554-4563, 10.1021/acs.est.5b06247,
792 2016.

793 Zhao, Y., Lambe, A. T., Saleh, R., Saliba, G., and Robinson, A. L.: Secondary organic aerosol
794 production from gasoline vehicle exhaust: Effects of engine technology, cold start, and emission
795 certification standard, Environmental science & technology, 52, 1253-1261, 2018.

796

797

Figure Caption

799 **Figure 1.** IVOC emission factors measured under different conditions, i.e. different

800   fuel type (gasoline, E10), test cycles (Chinese Light vehicles Test Cycle, CLTC,

801   and World-wide harmonized Light-duty Test Cycle, WLTC), starting mode (hot

802   start and cold start), and acceleration rates (acceleration rates of 1.2, 3.6 and 6.0

803   km/h/s). Stars indicate the EF data from US, i.e. median US LEV-2 gasoline

804   vehicles (vehicles manufactured in 2004-2012), non-road construction machinery,

805   and a large cargo vessel (Qi et al., 2019; Huang et al., 2018; Zhao et al., 2016).

806   The first category "China V" is the compilation of all the EF results from all of the

807   CLTC and WLTC tests. The boxes indicate the median value, with error bars

808   represent one standard deviation.

809 **Figure 2.** (a) Comparison of average chemical speciation of IVOC emissions from

810   China V vehicle and US vehicles (Zhao et al., 2016); (b) Average mass spectrum

811   of the IVOC during a typical E10-fueled cold start CLTC test. (c-d) Box-whisker

812   plots of the fractional contribution of selected fragments to total IVOCs signal for

813   tested China V vehicle：(c) B_{12}-B_{16} bins; (d) B_{17}-B_{22} bins. The boxes represent the

814   25th and 75th percentiles with the centerline being the median. The whiskers are the

815   10th and 90th percentiles. Black hollow triangles represent median LEV-2 data

816   from Zhao et al. [13] LEV-2 represents vehicles manufactured from 2004 to 2012.

817   Fragments colored in blue represent aliphatic compounds, while those colored in

818   orange are associated with aromatic compounds.

819 **Figure 3.** Comparison of IVOC volatility distributions of Chinses gasoline vehicle

820   exhaust, US gasoline vehicle exhaust, and Chinses E10 fuel. The box-plot

821   represents the Chinses gasoline vehicle exhaust. The boxes represent the 25th and

822   75th percentiles with the centerline being the median. The whiskers are the 10th and

823   90th percentiles. Red solid circles represent IVOC fractions of US vehicle exhaust

824   (Zhao et al., 2016). Blue hollow triangles represent the IVOCs volatility

825   distribution of Chinese E10 fuel. As all the studies performed in US used

826   commercial US gasoline as fuel, which contained 10% v/v ethanol, i.e. E10 fuel.

827   Therefore, we compare the Chinese E10 with US fuel to get a consistent

828   comparison. Also, we should note that Zhao et al. (2016) and Lu et al. (2018)

829   found that consistent distribution of US fuel and exhaust, so in this figure, the US

830   gasoline vehicle exhaust can represent the volatility distribution of its unburned

831   fuel distribution as well.

832   **Figure 4.** Comparison of emission factors of (a) PM (b) NO_x (c) THC, and (d) IVOC

833   between China and US on road gasoline vehicles (Zhao et al., 2016; May et al.,

834   2014). The boxes present the 75th and 25th percentiles with the centerline

835   represents being the median. The US vehicles are grouped by the model year, i.e.

836   pre-LEV refers to vehicles manufactured prior to 1994, LEV-1 represents vehicles

837   from 1994-2003, and LEV-2 is vehicles manufactured from 2004-2012.

838   **Figure 5** Comparison of POA and estimated SOA production after 48 h of

839   photo-oxidation (a) under low NO_x condition; (b) at an OA loading of 10 $\mu g \cdot m^{-3}$

840   under high NO_x condition; (c) at an OA loading of 20 $\mu g \cdot m^{-3}$ under high NO_x

841   condition; (d) at an OA loading of 80 $\mu g \cdot m^{-3}$ under high NO_x condition. The blue

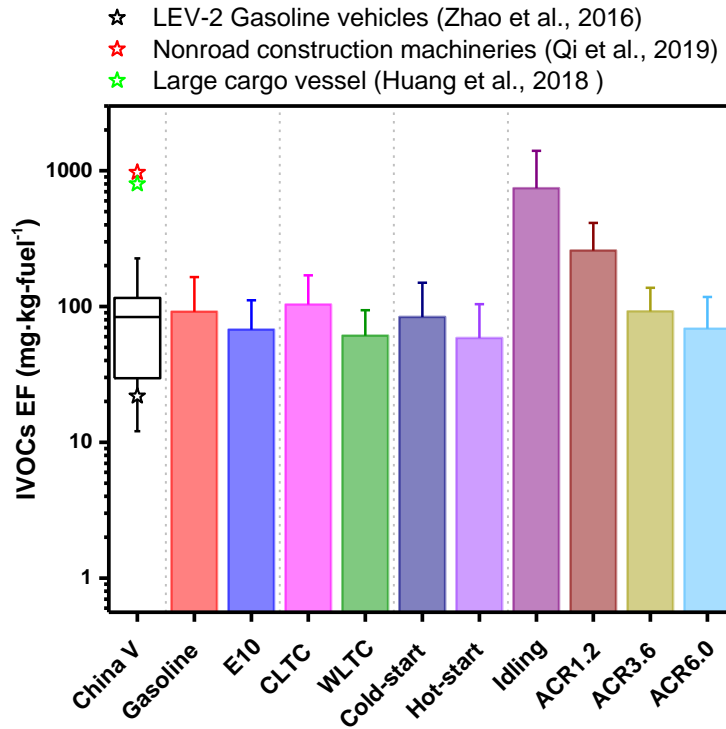842   circles represent the SOA-to-POA ratio after 48 h of photooxidation (right axis).

843

Figure 1. IVOC emission factors measured under different conditions, i.e. different fuel type (gasoline, E10), test cycles (Chinese Light vehicles Test Cycle, CLTC, and World-wide harmonized Light-duty Test Cycle, WLTC), starting mode (hot start and cold start), and acceleration rates (acceleration rates of 1.2, 3.6 and 6.0 km/h/s). Stars indicate the EF data from US, i.e. median US LEV-2 gasoline vehicles (vehicles manufactured in 2004-2012), non-road construction machinery, and a large cargo vessel (Qi et al., 2019; Huang et al., 2018; Zhao et al., 2016). The first category "China V" is the compilation of all the EF results from all of the CLTC and WLTC tests. The boxes indicate the median value, with error bars represent one standard deviation.
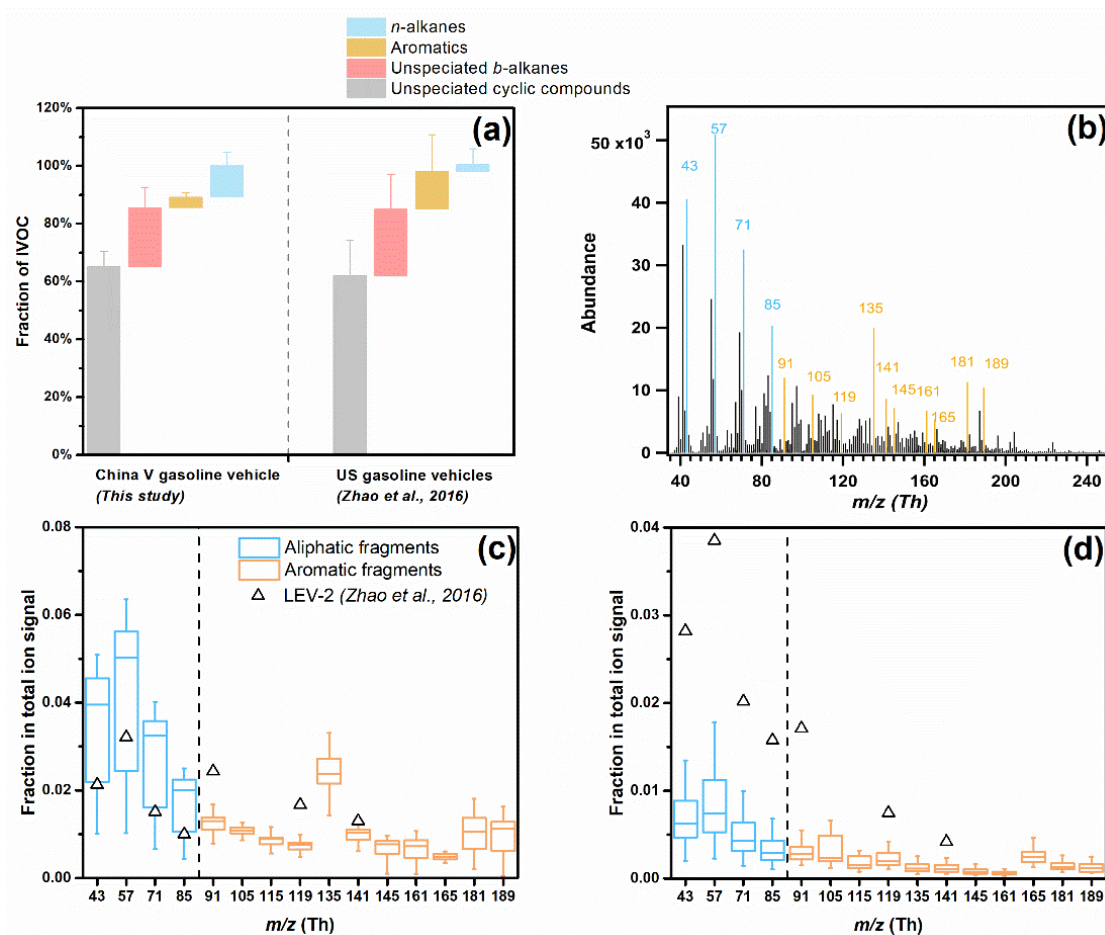
Figure 2. (a) Comparison of average chemical speciation of IVOC emissions from China V vehicle and US vehicles (Zhao et al., 2016); (b) Average mass spectrum of the IVOC during a typical E10-fueled cold start CLTC test. (c-d) Box-whisker plots of the fractional contribution of selected fragments to total IVOCs signal for tested China V vehicle：(c) B_{12}-B_{16} bins; (d) B_{17}-B_{22} bins. The boxes represent the 25th and 75th percentiles with the centerline being the median. The whiskers are the 10th and 90th percentiles. Black hollow triangles represent median LEV-2 data from Zhao et al. (2016) LEV-2 represents vehicles manufactured from 2004 to 2012. Fragments colored in blue represent aliphatic compounds, while those colored in orange are associated with aromatic compounds.
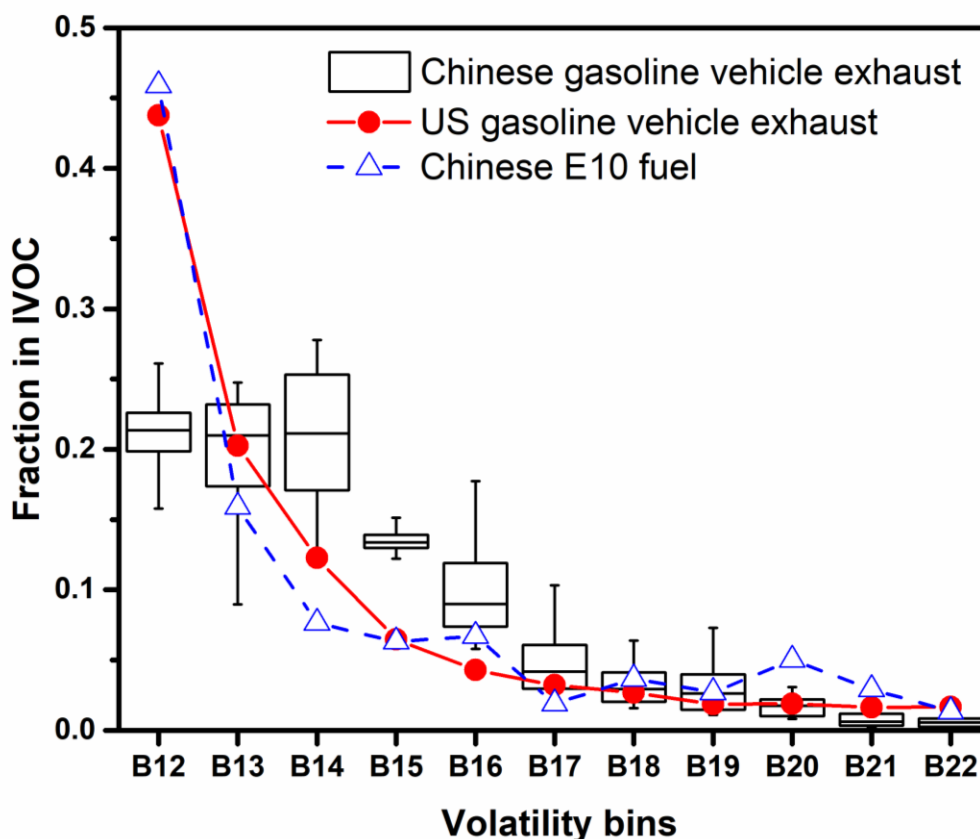
Figure 3. Comparison of IVOC volatility distributions of Chinses gasoline vehicle exhaust, US gasoline vehicle exhaust, and Chinses E10 fuel (ethanol volume ratio of 10%, v/v). The box-plot represents the Chinses gasoline vehicle exhaust. The boxes represent the 25th and 75th percentiles with the centerline being the median. The whiskers are the 10th and 90th percentiles. Red solid circles represent IVOC fractions of US vehicle exhaust (Zhao et al., 2016). Blue hollow triangles represent the IVOCs volatility distribution of Chinese E10 fuel. As all the studies performed in US used commercial US gasoline as fuel, which contained 10% v/v ethanol, i.e. E10 fuel. Therefore, we compare the Chinese E10 with US fuel to get a consistent comparison. Also, we should note that Zhao et al. (2016) and Lu et al. (2018) found that consistent distribution of US fuel and exhaust, so in this figure, the US gasoline vehicle exhaust can represent the volatility distribution of its unburned fuel distribution as well.
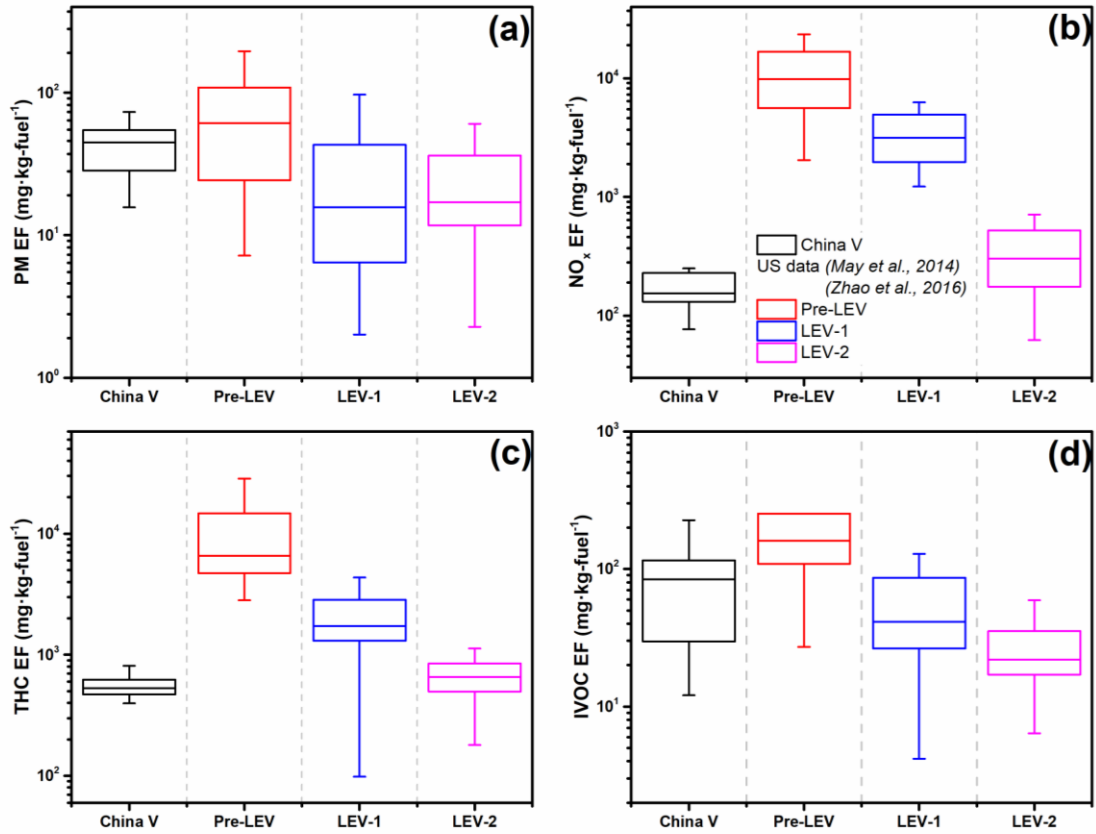
Figure 4. Comparison of emission factors of (a) PM (b) NO_x (c) THC, and (d) IVOC between China and US on road gasoline vehicles (Zhao et al., 2016; May et al., 2014). The boxes present the 75th and 25th percentiles with the centerline represents being the median. The US vehicles are grouped by the model year, i.e. pre-LEV refers to vehicles manufactured prior to 1994, LEV-1 represents vehicles from 1994-2003, and LEV-2 is vehicles manufactured from 2004-2012.
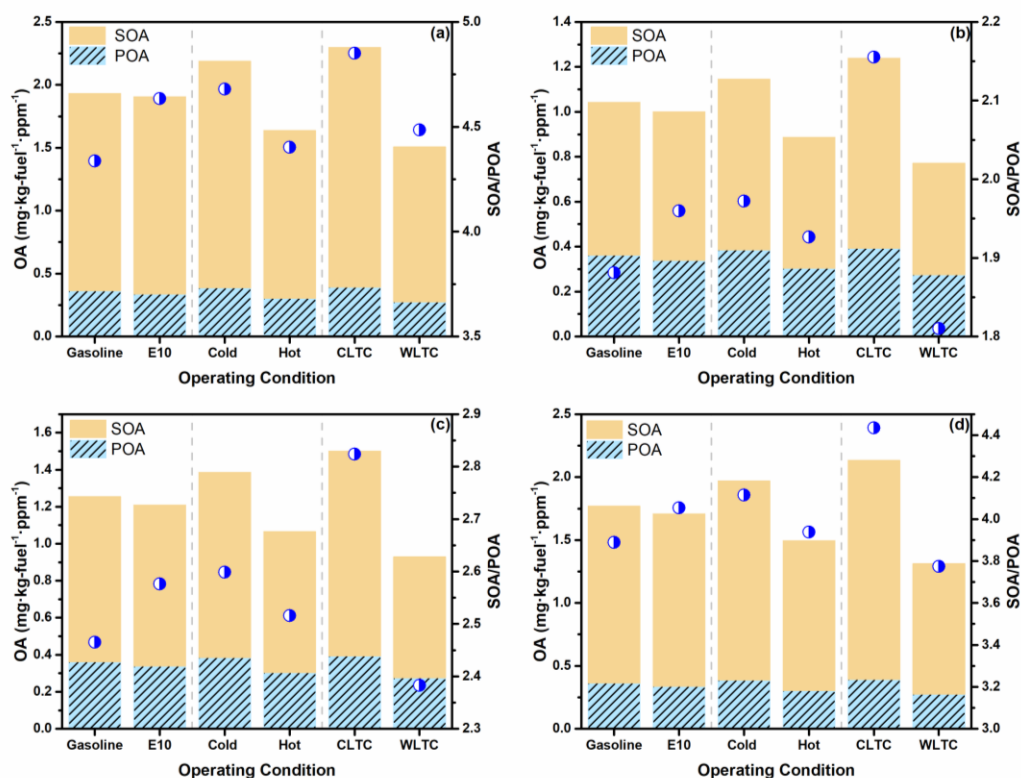
Figure 5 Comparison of POA and estimated SOA production after 48 h of photo-oxidation (a) under low NO_x condition; (b) at an OA loading of 10 $\mu g \cdot m^{-3}$ under high NO_x condition; (c) at an OA loading of 20 $\mu g \cdot m^{-3}$ under high NO_x condition; (d) at an OA loading of 80 $\mu g\ m^{-3}$ under high NO_x condition. The blue circles represent the SOA-to-POA ratio after 48 h of photooxidation (right axis).